CrystEngComm

A square-shaped complex with an electron-acceptor ligand: unique cubic crystal symmetry and similarity to inorganic mineral katoite

Journal:	*CrystEngComm*
Manuscript ID	CE-COM-07-2021-000994.R4
Article Type:	Paper
Date Submitted by the Author:	24-Sep-2021
Complete List of Authors:	Aoki, Kentaro; Kyoto University, Division of Chemistry, Graduate School of Science Otsubo, Kazuya; Kyoto University, Division of Chemistry Kitagawa, Hiroshi; Kyoto University, Department of Chemistry

ARTICLE

A square-shaped complex with an electron-acceptor ligand: unique cubic crystal symmetry and similarity to inorganic mineral katoite

Received 00th January 20xx,
Accepted 00th January 20xx

DOI: 10.1039/x0xx00000x

Kentaro Aoki,[a] Kazuya Otsubo*[a] and Hiroshi Kitagawa*[a]

Square macrocyclic complexes have attracted significant attention due to their unique structure and molecular recognition property. Here we report a square macrocyclic complex using an electron-acceptor ligand *N*,*N*′-di(4-pyridyl)-1,4,5,8-naphthalenediimide (dpndi), $[Pt(en)(dpndi)]_4(SO_4)_4{\cdot}20H_2O$ (**1**, en: ethylenediamine). Molecular structure of **1** was determined from single-crystal X-ray crystallography, and **1** is the largest Pt square (side: 2.6 nm) whose structure was crystallographically determined. **1** has an eight-electron-accepting property according to the electrochemical study. In **1**, the multiple interactions (hydrogen bonding and lone pair···π interaction) among the square units were observed in the solid state. This is in sharp contrast to the previous report of the square macrocyclic complexes since the square–square interactions were rarely observed in these structures. The multiple square–square interactions in **1** led to the symmetrical packing of the square units and crystallization in a unique cubic crystal symmetry. Moreover, the packing structure of **1** showed a strong similarity to the high-pressure phase of the natural mineral katoite.

Introduction

Macrocyclic complexes, obtained via self-assembly of metal sources and organic linkers, have attracted much interest in materials chemistry.[1] By tuning the coordination geometry around the metal centre including the shape of the organic linkers, various kinds of macrocyclic complexes such as triangles, squares and hexagons have been synthesized.[2] Among the macrocyclic complexes, the most investigated is the square-shaped macrocyclic complex due to the molecular recognition for aromatic molecules and inorganic ions.[3] In general, the square planar coordination geometry of d^8 divalent cations (Pt^{2+}, Pd^{2+}) and the rigid, linear organic bidentate linkers provide the selective and energetically favourable formation of the square macrocyclic complexes.[4] Based on this strategy, various kinds of square macrocyclic complexes with a variety of physical properties including chirality,[5a] redox activity[5b,c] and luminescence[5d] have been synthesized. Herein, we report the synthesis of a square macrocyclic complex using an electron-accepting ligand dpndi (Fig. 1(a)). The naphthalenediimide moiety of dpndi has two-electron-accepting property to form a radical anion and dianion (Fig. S1, ESI†).[6] Hence, introduction of dpndi can be expected for a square macrocyclic complex with an electron-accepting property. Self-assembly of the square macrocyclic complex was monitored using ^{1}H NMR measurement. The molecular structure of **1** was revealed by single-crystal X-ray diffraction analysis. This complex is the largest Pt square macrocyclic complex solved by crystallographic analysis. Moreover, introducing electron-accepting moiety leads to multiple interactions among the square units, resulting in a unique cubic crystal symmetry in the solid state. The packing structure of **1** shared the great similarity to the high-pressure phase of the inorganic mineral katoite $(Ca_3Al_2(SiO_4)_{3-x}(OH)_{4x}$, x = 1.5–3),[7] a type of hydrogrossular garnet.

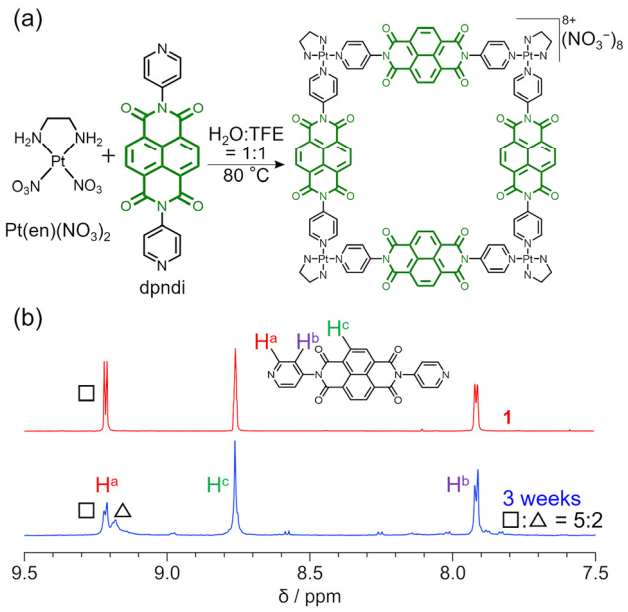

Fig. 1 (a) Synthetic scheme of the square macrocyclic complex $[Pt(en)(dpndi)]_4(NO_3)_8$. (b) Aromatic region of the ^{1}H NMR spectra of product after a 3-week reaction (blue) and anion exchanged to SO_4^{2-} (red) in DMSO-d_6.

[a] *Division of Chemistry, Graduate School of Science, Kyoto University, Kitashirakawa-Oiwakecho, Sakyo-ku, Kyoto, 606-8502, Japan.*

† Electronic Supplementary Information (ESI) available: Synthesis, structural analysis, cavity calculation and theoretical calculation. See DOI: 10.1039/x0xx00000x

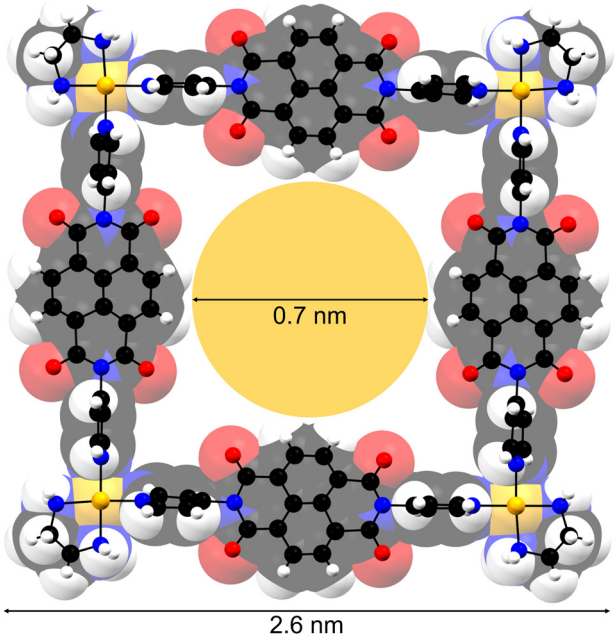

Fig. 2 Molecular structure of **1** at 100 K. One square unit is drawn using ball and stick with the CPK model. The side has 2.6 nm length, and void space exists inside the square with 0.7 nm diameter.

Table1. Crystallographic data for **1**.

Compound	**1**
Empirical formula	$C_{104}H_{80}N_{24}O_{16}S_4Pt_4{\cdot}68H_2O{\cdot}17THF$
Formula weight	5537.4
Temperature (K)	100(2)
Wavelength (Å)	0.71075
Crystal system	Cubic
Space group	*I*–43*d* (#220)
Unit cell dimensions (Å)	*a* = 39.9546(6)
Volume (Å^3)	63782(3)
Z	12
Density(calculated) (g/cm^3)	1.730
Absorption coefficient (mm^{-1})	2.711
F(000)	34368
Crystal size (mm^3)	0.42 × 0.34 × 0.26
Theta range for data collection (°)	3.5329 to 30.489
Reflection collected	239627
Independent reflections	15679 (R_{int} = 0.2307)
Completeness	99.6% (ϑ_{max} = 25.242°)
Absorption collection	Empirical
Refinement method	Full-matrix least-squares on F^2
Data / restraints / parameters	15679 / 53 / 166
Goodness-of-fit on F^2	0.983
$R_1{}^a$ [I>2σ(I)]	0.0664
$wR_2{}^b$ indices (all reflections)	0.2012
Largest diff. peak and hole (e/Å^3)	1.264 and –0.544
Flack parameter	0.03(1)

$^aR_1 = \Sigma||F_o| - |F_c||/\Sigma|F_o|$. $^bwR_2 = \{\Sigma w[(F_o)^2 - (F_c)^2]^2/\Sigma[w(F_o)^2]^2\}^{1/2}$.

Experimental section

Materials and Methods

K_2PtCl_4, en, $AgNO_3$, 1,4,5,8-naphthalene-tetracarboxylic dianhydride, 4-aminopyridine, K_2SO_4, $(Bu_4N)NO_3$, HNO_3, *N*,*N*′-dimethylformamide (DMF), tetrahydrofuran (THF), DMSO-d_6 (DMSO: dimethyl sulfoxide) and ethanol were purchased from Wako Pure Chemical Industries, Ltd.. 2,2,2-trifluoroethanol (TFE) was purchased from Nacalai Tesque Inc. All reagents and solvents were used without further purification. ^{1}H-NMR spectra were recorded using a Bruker AVANCE600 (Bruker) at room temperature. DMSO-d_6 (δ = 2.50) was used as a deuterated solvent. Elemental analysis was performed at Elemental Analysis Center, Faculty of Pharmaceutical Science of Kyoto University. Fourier transform infrared (FT-IR) spectra were recorded on ThermoNicolet NEXUS 670 FTIR Spectrometer (Thermo Fisher) at room temperature and diluted in KBr. The thermogravimetric analysis (TGA) was carried out using a TG-DTA 2000SA (Bruker AXS) at a heating rate of 2 K per min in a constant flow of N_2. Cyclic voltammetry (CV) measurements were performed in DMF solution with 0.05 mol/L $(Bu_4N)NO_3$ using a CHI 760e electrochemical workstation (CH Instruments, Inc.) connected with a RRDE-3A constant rotation system (ALS Co., Ltd) at room temperature. We used a conventional three-electrode system; namely, an Ag/Ag$^+$ reference electrode, a Pt wire counter electrode, and a glassy carbon electrode as a working electrode. The scan rate was 100 mV s^{-1}. Density functional theory (DFT) calculations including highest occupied molecular orbital (HOMO) and lowest unoccupied molecular orbital (LUMO) were carried out for ligand dpndi and **1**.

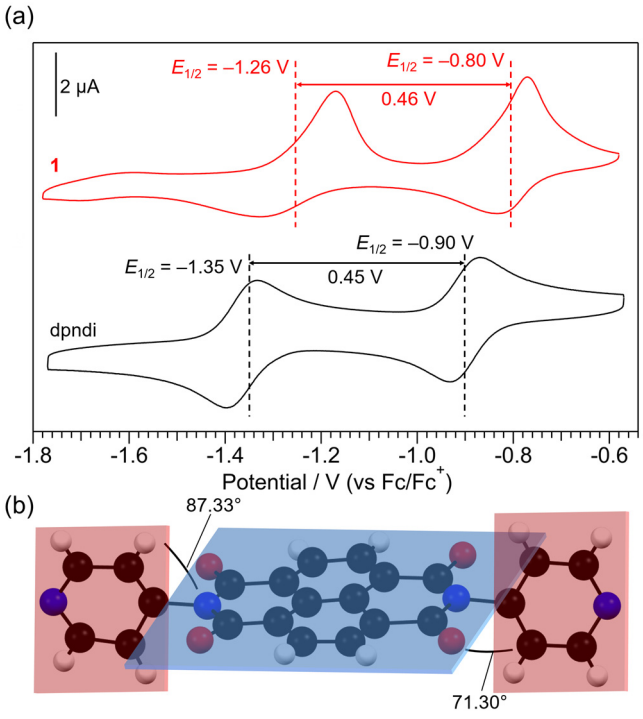

Fig. 3 (a) Cyclic voltammograms of dpndi (black) and **1** (red) in DMF. $E_{1/2}$ values and the difference of $E_{1/2}$, corresponding to the on-site Coulomb repulsion, is also shown. (b) Geometry of the electron-accepting moiety (blue plane) and pyridyl moieties (red planes) in **1**. The dihedral angles between blue and red plane are 87.33° and 71.30°.

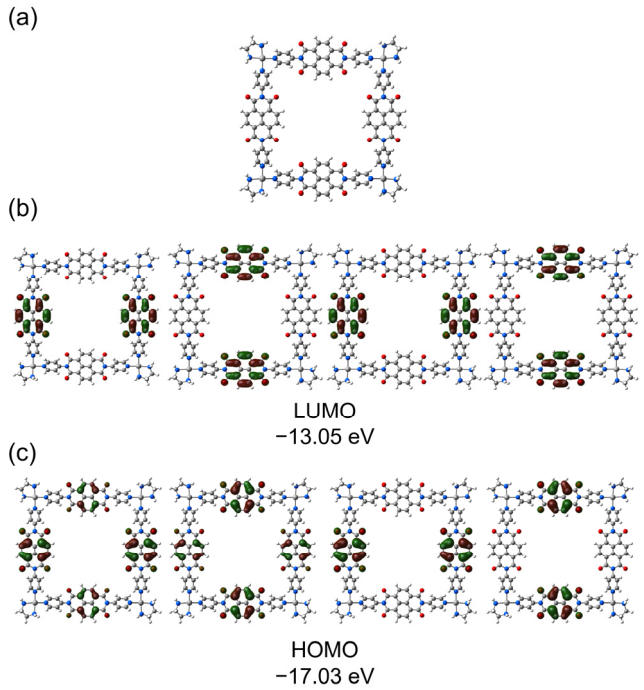

Fig. 4 (a) Optimized structure, (b) HOMO and (c) LUMO of **1**. Values below the orbitals denote the energy levels.

The calculation was performed with the PBEPBE1/GENECP level of theory using the 3-21g basis set for H, C, N and O atoms and the SDD (Stuttgart-Dresden) basis set for Pt atoms. The structure of dpndi was used according to the result of the single-crystal dpndi was used according to the result of the single-crystal X-ray study.[8] The geometries were fully optimized under no symmetry constraints for dpndi, whereas the D4 point symmetry was applied for 1. The natural population analysis was performed using natural bond orbital (NBO) calculations. All the computations were implemented with the Gaussian 09W program package.[9]

Synthesis of square macrocyclic complex, $[Pt(en)(dpndi)]_4(NO_3)_8$

Cis-capped Pt complex $Pt(en)(NO_3)_2$[10] and dpndi[11] were synthesized according to the previous report. An equimolar mixture of $Pt(en)(NO_3)_2$ (123 mg, 0.324 mmol) and dpndi (136 mg, 0.324 mmol) was dissolved in 17.8 mL of a 1:1 ratio of H_2O and TFE solution with 10 µL of HNO_3, and heated at 80 ˚C under reflux. After a 3-week reaction, the solution was filtered to remove the Pt black, and evaporated under reduced pressure to obtain 253 mg of the product (yield 88.2%).

Single-crystal X-ray crystallography

Single-crystal X-ray crystal structure analysis of **1** at 100 K was performed using a XtaLAB PRO (Rigaku, Japan) diffractometer equipped with a PILATUS3 R 200K-A detector with graphite monochromatized Mo *K*α radiation (λ = 0.71075 Å) under cold N_2 gas flow. Because the crystallinity decreased just after picking up from the mother liquid, the single crystal was mounted with some mother liquid onto MicroMeshes (MiTeGen) and quickly cooled under cold N_2 gas flow. The structure was solved using the direct method (SHELXT)[12] and expanded using Fourier techniques refined by the full-matrix least-squares technique on F^2 (SHELXL)[13] using the CrystalStructure[14] software package. It has a great amount of solvent-accessible area, and filled with highly disordered solvent molecules that could not be mapped by single-crystal X-ray diffraction. Thus, the SQUEEZE routine of PLATON[15] was applied to remove scattering contributions from solvent molecules. CCDC reference number: 2097475. Obtained crystallographic data was summarized in Table 1.

Results and discussion

Synthesis of compound 1

The synthetic scheme of the square macrocyclic complex $[Pt(en)(dpndi)]_4(NO_3)_8$ is shown in Fig. 1(a). The reaction was monitored at 1-week intervals using ^{1}H NMR (Fig. S2, ESI†) in DMSO-d_6. The blue line in Fig. 1b shows the ^{1}H NMR spectrum after a 3-week reaction. Three peaks were observed in the aromatic region, which can be assigned as H^a, H^b and H^c of dpndi. (See Fig. S3 for full range spectra.) The H^a peak splits into two peaks, which are assigned to the square and triangular macrocyclic complexes (See the geometric symbol in Fig. 1(b) and Fig. S4, ESI†.) based on the previous reports.[4a-4g] For H^b and H^c, the peaks of the square and triangular macrocyclic complexes heavily overlap. The integral ratio between the square and triangular macrocyclic complexes, calculated from H^a, was 5:2. Filtration and removal of the solvent under reduced pressure afforded the product with an 88% yield.

Structural determination

We tried various counter anions to crystallize the square macrocyclic complex, and found that anion exchange reaction to SO_4^{2-} yielded the crystals suitable for X-ray crystallography (Fig. S5, ESI†). The 3-week reaction product (5 mg) and K_2SO_4 (75 mg) were dissolved in 5 mL of a 4:1 ratio of H_2O and THF, and diffusion of ethanol afforded the yellow block-shaped crystals after 5 days at room temperature. The ^{1}H NMR spectrum clearly indicated the successful isolation of a square macrocyclic complex (red line of Fig. 1(b)). Single-crystal X-ray study at 100 K revealed the molecular structure of **1** (Fig. 2, see also Table 1 and Fig. S9, ESI†). Clear square structure was revealed, where the Pt^{II} ions and dpndi ligands are located at the vertex and side of the square unit, respectively. To the best of our knowledge, **1** is the largest square macrocyclic complex (side: 2.6 nm), structure of which was determined by the single-crystal X-ray structural analysis (see Fig. 5(e) to (h) for the previous Pt-based square macrocyclic complexes).

Electrochemical property

The electrochemical property of the isolated square macrocyclic complex **1** was investigated using CV in DMF. Two reversible reduction waves corresponding to the formation of the radical anion ($E_{1/2}$ = −0.80 V) and dianion ($E_{1/2}$ = −1.26 V) were observed against Fc/Fc^+ (Fc: ferrocene, red line in Fig. 3(a)), the same behaviour as dpndi (black line in Fig. 3(a), $E_{1/2}$ = −0.90 and −1.35 V). This corresponds to a total of eight-electron-accepting property per square unit in **1**. Understanding of the electronic structure of **1** was deepened by considering the difference of the $E_{1/2}$ values, corresponding to the on-site Coulomb repulsion energy. The on-site Coulomb repulsion energies of dpndi and **1** are 0.45 V and 0.46 V, respectively. These values are in fine agreement, indicating that the electronic structure of the electron-accepting moiety does not change even after the complexation. This can be understood from

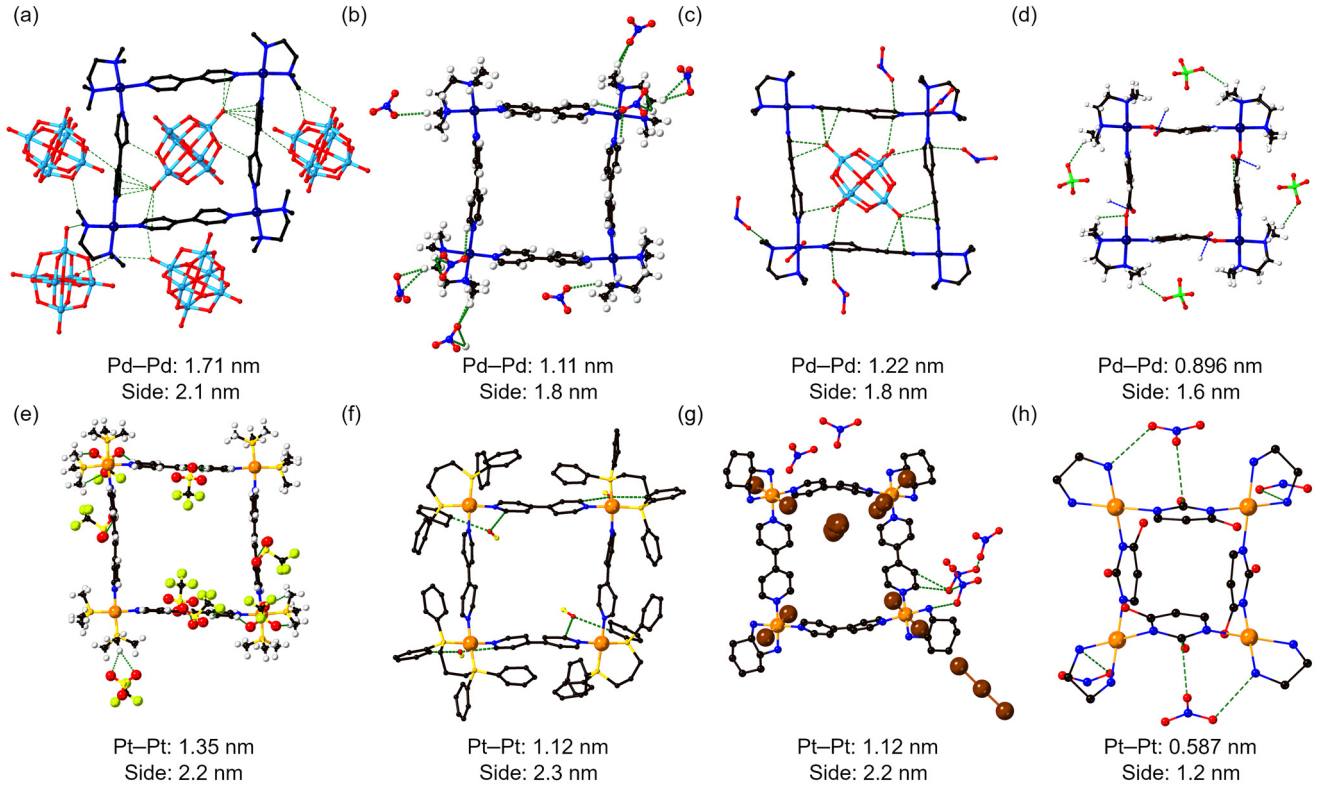

Figure 5. (a) to (d). Example of the Pd-based square macrocyclic complexes with the (a) triclinic (CCDC: 626151),[4j] (b) monoclinic (CCDC: 626150),[4j] (c) orthorhombic (CCDC: 626152)[4j] and (d) tetragonal (CCDC: 727403)[4k] crystal system, respectively. (e) to (h) Pt-based square macrocyclic complexes with the (e) triclinic (CCDC: 187314),[4g] (f) monoclinic (CCDC: 1308332),[4o] (g) orthorhombic (CCDC: 1441696)[4t] and (h) tetragonal (CCDC: 1201128)[4n] crystal system, respectively. Solvent molecules are omitted for clarity. Orange, Pt; light blue, W; navy, Pd; brown, Br; light green, Cl; yellow, P; yellow green, F; red, O; blue, N; black, C; white, H. Longest metal–metal distance and side length were denoted at the bottom. Green and blue dotted lines denote the short contacts between C–H···O and N–H···O (capping/bridging linker–anion) hydrogen bonding, and C–H···O (square–square) hydrogen bonding, respectively.

the structure of **1**. The electron-accepting moiety of **1**, located at the centre of dpndi, is almost perpendicular to the pyridyl unit in the solid state (Fig. 3(b)), and is inhibited to interact with other electron-accepting moieties or with Pt atoms. The DFT calculation further supported the isolated state of the electron-accepting moieties. Figure 4 shows the HOMO and LUMO of **1** (see Fig. S8 for HOMO and LUMO of dpndi). LUMO of **1** and dpndi is localized to the electron-accepting moieties and has no net interaction with each other or Pt atoms.

The square–square interactions and highly symmetrical packing

Surprisingly, **1** crystallized in a cubic space group, *I*–43*d*. Typically, square macrocyclic complexes obtained from *cis*-capped Pd^{2+} or Pt^{2+} crystallize in lower symmetric space groups, (11 triclinic, 4 monoclinic, 1 orthorhombic, and 2 tetragonal space groups, Fig. 5.).[4g-4q] The lower crystal symmetry arises from the poor interaction among the square units in the solid state. Hydrogen bondings between H atoms of capping/bridging linkers and counter anions are the dominant interactions (green dotted lines in Fig. 5), and there is little interaction among the square units (blue dotted lines in Fig. 5 (d)). This inhibits the symmetrical packing of the square units. By contrast, in **1**, multiple intermolecular interactions among the square units were revealed by the single-crystal X-ray study (Fig. 6). C–H···O (en–dpndi and dpndi–dpndi) and N–H···O (en–dpndi) hydrogen bondings (green dashed lines), and lone pair···π interactions (dpndi–dpndi, brown dashed lines) are clearly observed (Fig. 6(a), see also Fig. S10, ESI†). These multiple interactions contribute to the crystallization, in addition to the C–H···O (dpndi–SO_4^{2-}) hydrogen bonding (Fig. S10, ESI†). It should be noted that electron-accepting moiety plays a key role in square–square interactions. These square–square interactions were further examined using Hirshfeld surface analysis.[16] Figure 6(b) shows the Hirshfeld surface form of one square unit in **1**. The short contacts among the square units are clearly visualized. The surface shape and colour map imply that the lone pair···π interactions (brown circles, see also Fig. 6(a)) are important in the interaction with the adjacent square units.

Reflecting these interactions, the square units pack in a highly symmetrical manner, as shown in Fig. 7(a). For clarity, a schematic picture of the centre of gravity and square planes is shown. For one square unit (red), eight squares (blue and green) are located at the

nearest neighbour position. Four green squares approach to the void space of the red square from the up and down sides (4-in). On the other hand, four corners of the red square approach to the void space of the blue square units (4-out) (See also Fig. S12 and Supplementary Movie, ESI†). Moreover, blue and green squares follow the fourfold rotoreflection along the axis vertical to the red plane. This 4-in–4-out manner of the square packing with high symmetry resulted in crystallization in the cubic space group.

Packing structure with similarity to inorganic mineral katoite

Notably, the packing manner of **1** in the solid state shows a strong relation to the inorganic mineral katoite ($Ca_3Al_2(SiO_4)_{3-x}(OH)_{4x}$, x = 1.5–3), *vide infra*. The structure of the high-pressure phase (>5 GPa) with the space group *I*–43*d* is shown in Fig. 7(b).[17] Katoite consists of Ca, AlO_6 octahedra and SiO_4 tetrahedra, which can be classified as a type of garnet with SiO_4 partially replaced by OH. For the SiO_4 tetrahedron, there are two crystallographically independent sites (see the light green and sky blue tetrahedra in Fig. 7(b), (d) and (f)). In **1**, the centre of gravity of the square occupies the Wyckoff position 12b (0.000, 0.250, 0.875), which is the same as that of the right green SiO_4 tetrahedra (Fig. 7(d) and (e)). The centre of gravity of the two neighbouring SO_4^{2-} anions (S1, O5 and O6) occupies the 12a position (0.375, 0.000, 0.250), the same as the sky blue SiO_4 tetrahedra (Fig. 7(f) and (g)). Moreover, as shown in Fig. 7(h) and (i), the other SO_4^{2-} anion (S2, O7 and O8) occupies the Wyckoff position 16c (δ, δ, δ) (δ = −0.0220(4)), the same position as the AlO_6 octahedral site (ε, ε, ε) (ε = 0.0024).

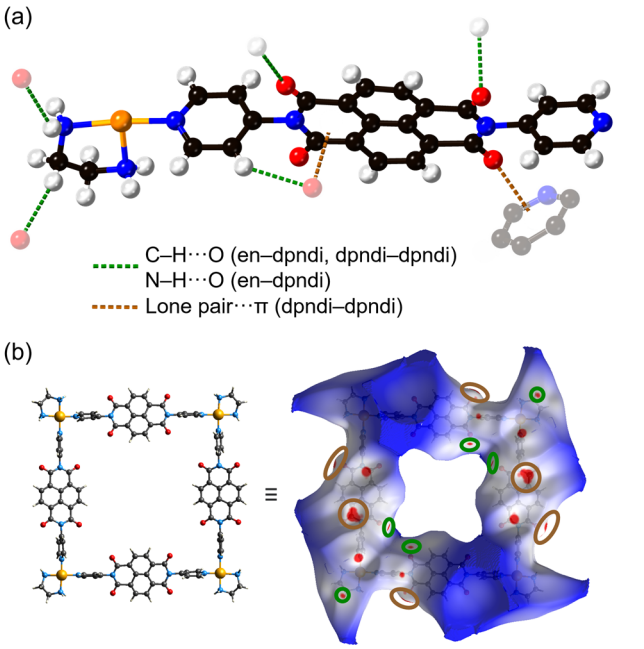

Fig. 6 (a) Asymmetric square unit of **1** (balls and solid lines) and short contact atoms (shaded balls). Short contacts among the square units can be divided into two, C–H···O (en–dpndi and dpndi–dpndi) and N–H···O (en–dpndi) hydrogen bondings (green dashed lines), and lone pair···π (dpndi–dpndi) interactions (brown dashed lines). (b) Hirshfeld surface view of one square unit. The Hirshfeld surface was mapped with d_{norm} over the range of –0.15 to 5.0, where d_{norm} is normalized contact distance. Red and blue parts denote the short and long contacts compared with the van der Waals contact, respectively. Short contacts corresponding to the green and brown dashed lines in panel (a) are depicted in green and brown circles, respectively.

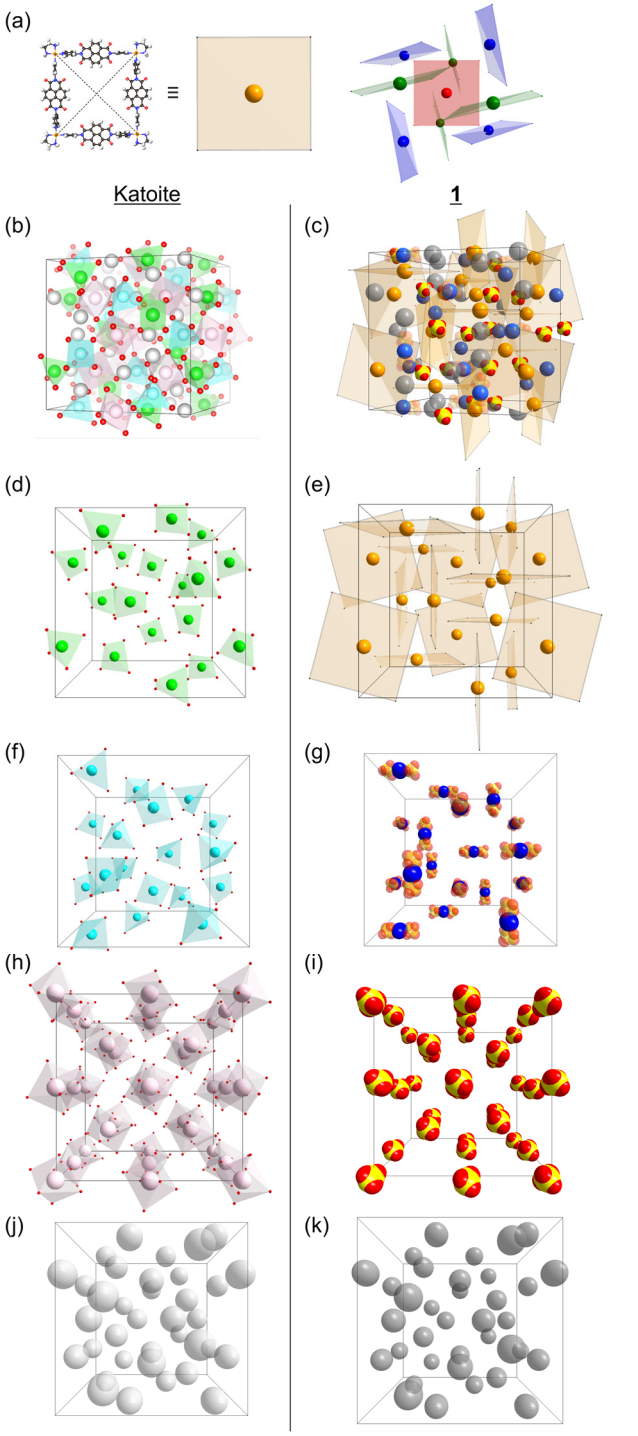

Fig. 7 (a) The packing of the square units in **1**. Only the square planes and the centre of gravity are shown for clarity. Four adjacent green square units approach to the void space of the red square unit (4-in), and the four corners of the red square unit approach the adjacent blue square units (4-out), with 4-in–4-out manner. (b) The packing structure of the high-pressure phase of katoite $Ca_3Al_2(SiO_4)_{3-x}(OH)_{4x}$ (x = 1.5–3). The crystallographic data was obtained from ref. 17(a), and drawn using VESTA.[18] Grey; Ca, pink; Al, light green and sky blue; Si, red: O. (c) The packing structure of **1**. (d) to (j) The packing structure of (d) one SiO_4 tetrahedra, (f) the other SiO_4 tetrahedra, (h) AlO_6 octahedra and (j) Ca of high-pressure phase of katoite. (e) to (k) The packing structure of (e) the centre of gravity of the square units, (g) one SO_4^{2-} anions and the centre of gravity of neighbouring SO_4^{2-}, (i) the other SO_4^{2-} anions and (k) cavity with a radius of 3.11 Å of **1**, from the crystallographic ***a***-axis with a perspective view.

Investigation of the cavity space of **1** provides further insight into similarities (Table S2, Figs. S13–S17, ESI†).[19] In the calculation of the cavity volume, the square units and SO_4^{2-} anions were considered, and the maximum sphere size that can fit the space was calculated for each cavity volume (Figs. S13–S17, ESI†). The cavity with a radius of 3.11 Å occupies 24d (0.138, 0.000, 0.250), whereas that of Ca is (0.134, 0.000, 0.250) (Fig. 7(j) and (k)). Strong similarity with one-to-one correspondence for each site was confirmed. Furthermore, this is the first example in which the analogy of the packing structure between a macrocyclic complex and an inorganic mineral is clarified.

Conclusions

In summary, a novel square macrocyclic complex **1** was synthesized using an electron-acceptor ligand, and its molecular structure was clarified by single-crystal X-ray structural analysis. **1** is the largest Pt square solved by crystallographic analysis. Moreover, **1** crystallizes in the unprecedented cubic crystal symmetry. Introduction of the electron-acceptor moiety leads to multiple intermolecular interactions among the square units, in the highly symmetrical 4-in–4-out manner. The packing structure of **1** shared similarity with the high-pressure phase of the natural mineral katoite.

Author contributions

K. O. and H. K. conceived and designed this study. K. A. contributed to all of the experimental works. K. A., K. O. and H. K. co-wrote the manuscript.

Conflicts of interest

There are no conflicts to declare.

Acknowledgements

This work was supported by Core Research for Evolutional Science and Technology (CREST) 'Creation of Innovative Functions of Intelligent Materials on the Basis of the Element Strategy', ACCEL from Japan Science and Technology Agency (JST), Grant-in-Aid for Specially Promoted Research (20H05623), and JSPS KAKENHI Grant Numbers JP20350030, JP23245012, JP15H05479, JP17H05366, JP19K05494, JP19H04572 (Coordination Asymmetry) and JP19J23310 (JSPS Research Fellowships for Young Scientists).

Notes and references

1 (a) T. R. Cook and P. J. Stang, *Chem. Rev.*, 2015, **115**, 7001; (b) B. J. Holliday and A. C. Mirkin, *Angew. Chem., Int. Ed.*, 2001, **40**, 2022; (c) R. Chakrabarty, P. S. Mukherjee and P. J. Stang, *Chem. Rev.*, 2011, **111**, 6810; (d) A. Kumar, S.-S. Sun and A. J. Lees, *Coord. Chem. Rev.*, 2008, **252**, 922.

2 (a) M. Fujita, *Chem. Soc. Rev.*, 1998, **27**, 417; (b) S. J. Lee and J. T. Hupp, *Coord. Chem. Rev.*, 2006, **250**, 1710; (c) M. Fujita, M. Tominaga, A. Hori and B. Therrien, *Acc. Chem. Res.*, 2005, **38**, 371; (d) M. Fujita, *Coord. Chem. Rev.*, 1998, **27**, 417; (e) M. Yoshizawa, M. Nagao, K. Kumazawa and M. Fujita, *J. Organomet. Chem.*, 2005, **690**, 5383. (f) R. Hashiguchi, K. Otsubo, H. Ohtsu, H. Kitagawa, *Chem. Lett.* 2013, **42**, 374; (g) K. Aoki, K. Otsubo, G. S. Hanan, K. Sugimoto, H. Kitagawa, *Inorg. Chem.* 2018, **57**, 6222.

3 (a) M. Fujita, J. Yazaki and K. Ogura, *J. Am. Chem. Soc.*, 1990, **112**, 5645; (b) P. J. Stang and B. Olenyuk, *Acc. Chem., Res.*, 1997, **30**, 502; (c) M. Fujita and K. Ogura, *Bull. Chem. Soc. Jpn.*, 1996, **69**, 1471; (d) M. Fujita, J. Yazaki and K. Ogura, *Tetrahedron Lett.*, 1991, **32**, 5589; (e) M. Fujita, S. Nagao, M. Iida, K. Ogata and K. Ogura, *J. Am. Chem. Soc.*, 1993, **15**, 1574; (f) M. Fujita, F. Ibukuro, H. Hagihara and K. Ogura, *Nature*, 1994, **367**, 720.

4 (a) M. Ferrer, A. Gutiérrez, M. Mounir, O. Rossell, E. Ruiz, A. Rang and M. Engeser, *Inorg. Chem.*, 2007, **46**, 3395; (b) M. Ferrer, A. Pedrosa, L. Rodríguez, O. Rossell and M. Vilaseca, *Inorg. Chem.*, 2010, **49**, 9438; (c) M. Schweiger, S. R. Seidal, A. M. Arif and P. J. Stang, *Inorg. Chem.*, 2002, **41**, 2556; (d) M. Ferrer, M. Mounir, O. Rossell, E. Ruiz and A. Maestro, *Inorg. Chem.*, 2003, **42**, 5890; (e) T. Weilandt, R. T. Troff, H. Rissanen and C. A. Schalley, *Inorg. Chem.*, 2008, **47**, 7588; (f) S. B. Lee, S. Hwang, D. S. Chung, H. Yun and J.-I. Hong, *Tetrahedron Lett.*, 1998, **39**, 873; (g) M. Schweiger, S. R. Seidel, H. Saxell, K. Rissanen and C. A. Schalley, *Inorg. Chem.*, 2008, **47**, 7588; (h) M. Fujita, O. Sasaki, T. Mitsuhashi, T. Fujita, J. Yazaki, K. Yamaguchi and K. Ogura, *Chem. Commun.*, 1996, 1535; (i) J. A. Whiteford, C. V. Lu and P. J. Stang, *J. Am. Chem. Soc.*, 1997, **119**, 2524; (j) K. Uehara, K. Sakai, and N. Mizuno, *Inorg. Chem.*, 2007, **46**, 2563; (k) S. Ghosh and P. S. Mukherjee, *Inorg. Chem.*, 2009, **48**, 2605; (l) B. Roy, R. Saha, A. K. Ghosh, Y. Patil and P. S. Mukherjee, *Inorg. Chem.*, 2017, **56**, 3579; (m) K.-i. Otake, K. Otsubo, T. Komatsu, S. Dekura, J. M. Taylor, R. Ikeda, K. Sugimoto, A. Fujiwara, C.-P. Chou, A. W. Sakti, Y. Nishimura, H. Nakai and H. Kitagawa, *Nat. Commun.*, 2020, **11**, 843; (n) H. Rauter, E. C. Hillgeris, A. Erxleben and B. Lippert, *J. Am. Chem. Soc.*, 1994, **116**, 616; (o) P. J. Stang, D. H. Cao, S. Saito and A. M. Arif, *J. Am. Chem. Soc.*, 1995, **117**, 6273; (p) S. Shanmugaraju, A. K. Bar, K.-W. Chi and P. S. Mukherjee, *Organometallics*, 2010, **29**, 2971; (q) P. J. Stang, B. Olenyuk, J. Fan and A. M. Arif, *Organometallics.*, 1996, **15**, 904; (r) M. A. Gordillo, P. A. Benavides and S. Saha, *Cryst. Growth Des.*, 2019, **19**, 6017. (s) J. A. Whiteford and P. J. Stang, *Inorg. Chem.*, 1998, **37**, 5595; (t) M. Fujita, J. Yazaki and K. Ogura, *Chem. Lett.*, 1991, **20**, 1031. (t) P. J. Stang and D. H. Cao, *J. Am. Chem. Soc.*, 1994, **116**, 4981; (u) K.-i. Otake, K. Otsubo, K. Sugimoto, A. Fujiwara and H. Kitagawa, *Angew. Chem., Int. Ed.*, 2016, **55**, 6448; (v) P. J. Stang, K. Chen and A. M. Arif, *J. Am. Chem. Soc.*, 1995, **117**, 8793;

5 (a) C. Müller, J. A. Whiteford and P. J. Stang, *J. Am. Chem. Soc.*, 1998, **120**, 9827; (b) F. Würthner and A. Sautter, *Org. Biomol. Chem.*, 2003, **1**, 240; (c) F. Würthner, and A. Sautter, *Chem. Commun.*, 2000, 445; (d) C. M. Darn and J.-M. Lehn, *J. Chem. Soc., Chem. Commun.*, 1994, 2313.

6 (a) G. Andric, J. F. Boas, A. M. Bond, G. D. Fallon, K. P. Ghiggino, C. F. Hogan, J. A. Hutchison, M. A.-P. Lee, S. J. Langford, J. R. Pilbrow, G. J. Troup and C. P. Woodward, *Aust. J. Chem.*, 2004, **57**, 1011; (b) Y. Fujiki, S. Shinkai and K. Sada, *Cryst. Growth Des.*, 2009, **9**, 2751; (c) S. Guha, F. S. Goodson, L. J. Corson and S. Saha, *J. Am. Chem. Soc.*, 2012, **134**, 13679; (d) S. Guha, F. S. Goodson, R. J. Clark and S. Saha, *CrystEngComm*, 2012, **4**, 1213; (e) Y. Zhou and L. Han, *Coord. Chem. Rev.*, 2021, **430**, 213655.

7 (a) E. Passaglia and R. Rinaldi, *Bull. Mineral.*, 1984, **107**, 605; (b) M. Sacerdoti and E. Passaglia, *Bull. Mineral.*, 1985, **108**, 1; (c) P. Adhikari, C. C. Dharmawardhana and W.-Y. Ching, *J. Am. Ceram. Soc.*, 2017, **100**, 4317.

8 J. Mizuguchi, T. Makino, Y. Imura, H. Takahashi and S. Suzuki, *Acta Crystallogr*., 2015, **E61**, 3044.
9 M. J. Frisch, G. W. Trucks, H. B. Schlegel, G. E. Scuseria, M. A. Robb, J. R. Cheeseman, G. Scalmani, V. Barone, B. Mennucci, G. A. Petersson, H. Nakatsuji, M. Caricato, X. Li, H. P. Hratchian, A. F. Izmaylov, J. Bloino, G. Zheng, J. L. Sonnenberg, M. Hada, M. Ehara, K. Toyota, R. Fukuda, J. Hasegawa, M. Ishida, T. Nakajima, Y. Honda, O. Kitao, H. Nakai, T. Vreven, J. A. Montgomery, Jr, J. E. Peralta, F. Ogliaro, M. Bearpark, J. J. Heyd, E. Brothers, K. N. Kudin, V. N. Staroverov, R. Kobayashi, J. Normand, K. Raghavachari, A. Rendell, J. C. Burant, S. S. Iyengar, J. Tomasi, M. Cossi, N. Rega, J. M. Millam, M. Klene, J. E. Knox, J. B. Cross, V. Bakken, C. Adamo, J. Jaramillo, R. Gomperts, R. E. Stratmann, O. Yazyev, A. J. Austin, R. Cammi, C. Pomelli, J. W. Ochterski, R. L. Martin, K. Morokuma, V. G. Zakrzewski, G. A. Voth, P. Salvador, J. J. Dannenberg, S. Dapprich, A. D. Daniels, O. Farkas, J. B. Foresman, J. V. Ortiz, J. Cioslowski and D. J. Fox, *Gaussian 09*, , Gaussian, Inc., Wallingford CT, 2009.
10 M. Fujita, J. Yazaki and K. Ogura, *Chem. Lett.*, 1991, **20**, 1031.
11 J.-Z. Liao, C. Wu, X.-Y. Wu, S.-Q. Denga and C.-Z. Lu, *Chem. Commun.*, 2016, **52**, 7394.
12 G. M. Sheldrick, *Acta Crystallogr*., 2015, **A71**, 3.
13 G. M. Sheldrick, *Acta Crystallogr*, 2008, **A64**, 112.
14 CrystalStructure 4.3.2: Crystal Structure Analysis Package, Rigaku Corporation, Tokyo, Japan.
15 A. L. Spek, *Acta Crystallogr.*, 2015, **C71**, 9.
16 M. J. Turner, J. J. McKinnon, S. K. Wolff, D. J. Grimwood, P. R. Spackman, D. Jayatilaka and M. A. Spackman, CrystalExplorer17 (2017). University of Western Australia.
17 (a) G. A. Lager, R. T. Downs, M. Origlieri and R. Garoutte, *Am. Mineral.*, 2002, **87**, 642; (b) A. Erba, A. M. Navarrete-López, V. Lacivita, P. D'Arco and C. M. Zicovich-Wilson, *Phys. Chem. Chem. Phys.*, 2015, **17**, 2660; (c) G. A. Lager and R. B. Von Dreele, *Am. Mineral.*, 1996, **87**, 642.
18 K. Momma and F. Izumi, *J. Appl. Crystallogr.*, 2011, **44**, 1272.
19 D. C. Palmer (2014). *CrystalMaker*, CrystalMaker Software Ltd, Begbroke, Oxfordshire, England.